LAWRENCE
LIVERMORE
NATIONAL
LABORATORY

UCRL-JRNL-218359

# ToF-SIMS study of polycrystalline uranium after exposure to deuterium

P. Morrall, D. Price, A. Nelson, W. Siekhaus, E. Nelson, K. J. Wu, M. Stratman, B. McLean

January 24, 2006

Philosophical Magazine

## Disclaimer

UCRL-JRNL-218359

# ToF-SIMS study of polycrystalline uranium after exposure to deuterium

P. Morrall[1]*, D.W. Price[1], A.J. Nelson[2], W.J. Siekhaus[2], E. Nelson[2], K.J. Wu[2], M. Stratman[2] and W. McLean II[2]

[1]*AWE, Aldermaston, Reading, Berkshire, RG7 4PR, UK*

[2]*Lawrence Livermore National Laboratory, 7000 E Avenue, Livermore, CA 94550, USA*

*email : peter.morrall@awe.co.uk
Tel : +44 118 982 5842
Fax : +44 118 982 5024

## Abstract

Time-of-flight secondary ion mass spectrometry (ToF-SIMS) is employed to examine specific features observed on a polycrystalline depleted uranium sample after exposure to high purity $D_2$ gas. The ToF-SIMS investigation, being the first of its kind on uranium, investigates a site where the deuterated form of uranium hydride ($UD_3$) is clearly observed to have broken through the thin, air-formed oxide. Density functional theory calculations have been performed, which confirm the stability of, and also assign structural geometries to, the various uranium containing fragments observed with SIMS. An inclusion site was also investigated using ToF-SIMS, and these data suggest that the edges of such inclusions exhibit increased D ion, and hence H ion, diffusion when compared to the surrounding surface oxide. These results offer support to the previously published hypotheses that inclusion sites on uranium surfaces exhibit an increased probability to form hydride sites under $H_2$ exposure.

**PACS codes** - 82.80.Rt, 82.80.Ms, 71.15.Mb, 81.05.Je

## Introduction

Understanding the factors which influence the initial formation, and development, of hydride sites on uranium metal surfaces under exposure to hydrogen gas is of paramount importance across many areas of the nuclear industry. The majority of these factors relate to the safe use and handling of uranium components and waste, since uranium hydride ($UH_3$) is highly pyrophoric, its formation affects the strength and ductility of uranium metal components, and due to the large volume expansion experienced when $UH_3$ forms serious physical deformations can occur [1].

The controlling factors behind hydride site initiation are still unclear, although many articles have been published in the literature that investigate the role which surface features and defects on $\alpha$-uranium, and its oxide overlayer, play in controlling hydride formation [2-5]. A variety of surface features such as grain boundaries, twins and inclusions have all been investigated as to there affect on hydride initiation [5, and references therein]. Strong correlations have also been observed between hydride attack and inclusions, as discussed by *Owen* and *Scudamore* [6]. Carbide features are commonly observed in $\alpha$-uranium, usually as cubic UC inclusions, although these features are also known to occur containing various trace elements [7].

In this article, an investigation employing time-of-flight secondary ion mass spectrometry (ToF-SIMS) is undertaken into the solid state reaction products formed after a hydride (or deuteride) site is exposed to air. In addition, an attempt is made to elucidate some of the influential factors in causing hydride sites to occur at specific locations across the uranium surface, and in particular with regard to surface inclusions. To further understand the stability of the ion fragments observed with ToF-SIMS, theoretical calculations have been performed using density functional theory (DFT). These calculations also give insight into the geometric structures adopted by uranium hydride ion fragments,

and although based on U-H species not U-D, the two systems are expected to be equivalent as regards structure.

## Experimental

A high purity polycrystalline depleted uranium coupon, approximately 3 g in weight, was employed for these experiments. The manufacture of the coupon involved careful annealing which resulted in a relatively large grain size (average grain diameter ≈ 100 μm). The uranium coupon was prepared by hand lapping using successively finer grit silicon carbide polished pads, with a final mechanical polish using a Syntron vibratory polisher and 1 μm diamond polishing solution. Subsequent, brief electro-polishing was undertaken in order to visually expose the details of the grain structure. The coupon was moved into the gas dosing apparatus and evacuated to a pressure of approximately $10^{-6}$ mbar as quickly as possible after completing the polishing process, with the total air exposure time after polishing not exceeding 3 minutes. The gas dosing apparatus was equipped with a Nikon SMZ1500 stereo-microscope and CCD camera to enable the progress of the hydriding reaction to be monitored and images to be periodically captured of the sample surface. The $D_2$ gas was supplied to the gas dosing apparatus from a 99.99 % purity $D_2$ gas bottle, through a Johnson Matthey HP-10 Hydrogen Purifier system resulting in $D_2$ with less than one part per $10^9$ of impurity gases. Exposure of the uranium coupon to $D_2$ gas was carried out under static pressure conditions at 2 bar for a total of 4.5 hours, equivalent to a dose of approximately $3 \times 10^{13}$ L (where 1 L = $10^{-6}$ Torr s). At the completion of the desired $D_2$ gas dose the sample was again evacuated to $10^{-6}$ mbar. A vacuum of $10^{-6}$ mbar should thermodynamically drive any $UH_3$ formed towards de-hydriding, however the kinetics of such a reaction are expected to be very slow in comparison with the time-scale employed, as demonstrated by *Condon* and *Larson* [8].

The ToF-SIMS measurements were undertaken using a Physical Electronics TRIFT III spectrometer equipped with a Au liquid metal ion source operating at

an energy of 22 keV. During these measurements, the ToF-SIMS instrument achieved an average mass resolution of approximately 3000, and a lateral resolution of around 1 μm. The Au ion source was optimised for single Au atom particles, rather than higher order Au clusters. However, the Au ion source could also be operated in a DC mode, allowing surface sputtering of samples and hence a depth profiling capability.

Stopping and range of ions in matter (SRIM) calculations have been undertaken which predict the sputtering efficiency of $UO_2$ using 22 keV Au ions at 45° incidence to be 6.4 U atoms / Au ion and 22 O atoms / Au ion. The SRIM calculations have been used in this article to calculate the approximate sputtering depths probed during DC sputter profiling with the Au liquid metal ion source. Such calculations are fraught with potential errors, since the sputtering efficiency is heavily dependent on the values selected for the surface binding energies of atoms within the material being sputtered. The values chosen for the surface binding energies within these calculations are the default values within the SRIM software. The errors which result from such calculations can be considerable, although the values reported in this article are intended to act as a guide to the reader, and not as absolute values.

The small molecular ions observed in these ToF-SIMS experiments are quite amenable to quantum mechanical analysis. In order to aid assignment of the SIMS data and to aid the understanding of why some molecular ions form while others do not, DFT calculations were undertaken on a number of molecular ions. These calculations were carried out using Gaussian03 [9] revision C.02 on dual Pentium IV processor nodes of a Beowolf cluster in 2-way SMP mode. Initial guesses for the wavefunction were supplied by Extended Hückel calculations within the program. PBE [10], the gradient-corrected pure DFT functional for both exchange and correlation, was used in all cases. The geometries and energies for the species with all of the reasonable spin states were calculated, and energetic analysis was carried out on the most stable. When calculations

converged on a non-*auf bau* electronic configuration, the offending orbitals were exchanged and the calculation repeated. This procedure was continued until a true ground-state was found with *auf bau* occupancy. All calculations were undertaken without the aid of symmetry except where stated. To aid convergence of the wavefunction, virtual orbitals were initially shifted by 0.01 Ha.

**Results and Discussion**

Figure 1 is an optical microscope image, taken directly after the 2 bar $D_2$ gas exposure, showing a $UD_3$ reaction site approximately 300 μm in diameter. Metal grain boundaries remain visible in figure 1, and are observed in the areas surrounding the $UD_3$ feature. Following the formation of this deuteride feature the sample was transferred, through air, to the ToF-SIMS instrument. During this initial air exposure small sparks of light were observed from the sample and explained as the pyrophoric deuteride reacting with oxygen in the air. The time taken to transfer the uranium coupon from the gas dosing apparatus to high vacuum in the ToF-SIMS instrument was less than 5 minutes. However, all visible reaction of the deuteride occurred within the first few seconds of this transfer period.

Figure 2 (total) shows the absolute positive ion image collected from the deuteride site shown in figure 1. For comparison it should be noted that figure 1 must be rotated 45° counter-clockwise to obtain the same orientation as seen in figure 2. It is clear to see that although the deuteride site has undergone slight changes between the optical image in figure 1 and the SIMS image in figure 2 (total), the feature maintains the same general appearance and size. The minor changes in shape are attributed to the fact that the optical microscope directly images the exposed deuteride, whereas the SIMS images are of the deuteride site after it has reacted with $O_2$ during the air transfer to the SIMS instrument. Indeed, the $UO_2^+$ (m/z = 270) image obtained prior to sputtering (not shown) shows equivalent intensity across the deuteride site and the surrounding areas, since the air oxidation has resulted in the surface of the deuteride site converting

to $UO_2$. Figure 3 shows the SIMS spectra captured from $UO_2$ outside the deuteride spot (top) and above the deuteride site (bottom). Both spectra show the characteristic secondary ion fragments expected from $UO_2$ with m/z = 238 ($U^+$), 254 ($UO^+$) and 270 ($UO_2^+$), although m/z = 239, 255 and 271 are also observed and interpreted as the recombination of $UO_2$ fragments with surface H to give $UH^+$, $UOH^+$ and $UO_2H^+$ respectively. The data taken away from the deuteride feature (top) show further additional lines at m/z = 257 and 273, which are interpreted as $UF^+$ and $UOF^+$ respectively, since otherwise these fragments could only be interpreted as either $UOHD^+$ or $UOH_3^+$ for m/z = 257 and $UO_2HD^+$ or $UO_2H_3^+$ for m/z = 273, which in both cases should also show peaks at m/z = 256 and 272, and these are not observed. The fluorine related peaks are not observed on the $UO_2$ found above the deuteride site since this formed at the instant when the deuteride reacted with air during the move into the SIMS instrument, and no fluorine would be expected to be present in either the hydride or air environments. Further evidence to support the assignment of the m/z = 257 and 273 peaks to fluorine contamination arises because these features are observed to quickly disappear with only gentle, large area, DC sputtering. If the peaks had been due to deuterium within the surface $UO_2$, then we would expect the deuterium related peaks to remain, at least to some extent, until the metal/oxide interface were reached. This large area DC sputtering is estimated through SRIM calculations to have penetrated less than 10 Å into the oxide surface layer, and therefore will certainly not have reached the metal/oxide interface.

Figure 2 ($UO_2^+$, $U^+$, $UD^+$, $D^-$, $UD_2^-$, $UD_3^-$ and $UD_4^-$) shows images captured after two 50 × 50 μm regions have been DC sputter etched into the surface. The first 50 × 50 μm sputtered area is at the top left of the images, and positioned away from the deuteride feature; the second 50 × 50 μm sputtered area is positioned atop of the deuteride feature. This more highly focused DC sputtering beam is estimated to penetrate 100 times deeper into the surface $UO_2$ than the gentle, large area sputtering undertaken previously. SRIM calculations estimate that the

depth of these two DC sputtered areas is approximately 700 Å deep. Figure 2 clearly shows a reduction of $UO_2^+$ intensity at both 50 × 50 μm sputter sites, with a relative increase in $U^+$ intensity on the area away from the deuteride feature, a slight increase in the $U^+$ intensity atop of the deuteride feature, and a significant intensity hot-spot observed for $UD^+$, $D^-$, $UD_2^-$, $UD_3^-$ and $UD_4^-$ at the sputtered site atop of the deuteride feature. The observation of $D^-$, $UD^+$, $UD_2^-$, $UD_3^-$ and $UD_4^-$ all provide irrefutable evidence of the presence of the deuterated form of uranium hydride, $UD_3$. These results clearly show that although the deuteride site has oxidised upon exposure to air, the oxidation appears to have terminated after the formation of a protective uranium oxide cap over the deuteride site. The thickness of the protective uranium oxide cap is estimated to be approximately 200 Å thick, based on the applied DC sputtering times and SRIM calculations.

Figure 4 shows the positive ion (bottom) and negative ion (top) SIMS spectra obtained from the sputter exposed deuteride region, with the assigned ion fragments shown above the data sets. Five major ion fragments are observed between m/z = 238 and 246, which are unambiguously assigned to $UD_3$. The other major ion fragments ($254 \leq m/z \leq 270$) are attributed to deuteride fragments combining with oxygen ions. These oxygen containing fragments probably occur from two competing recombination effects. Firstly from the recombination of secondary deuteride ions with oxygen ions extracted from within the walls of the sputtered recess to the deuteride site, and secondly due to oxygen from the gas phase which reacts with the highly active deuteride surface prior to being extracted by the ToF-SIMS instrument.

Table 1 gives the calculated ion energies for all the DFT species examined within the theoretical section of this article. Figure 5 shows the calculated geometries of the positive and negative $UH_x$ molecular ions obtained through DFT calculations. The $UH_2^{+/-}$ ions both adopt the linear arrangement of atoms with the uranium atom central. In the case of the $UH_3$ and $UH_4$ ions however, the structures adopted depend upon the charge of the ions, with the negatively

charged ions adopting structures based on a square planar geometry, and the positively charged ions adopting structures based on a tetrahedral geometry (with one position vacant in each case for the $UH_3$ ions). The U-H bond lengths are greater by approximately 0.20 Å in the case of the negatively charged molecular ions, when compared to the equivalent positive ions.

The calculations here are in slight contrast to the results of *Souter et al* [11], where it was found that an uncharged $UH_2$ molecule adopted a $C_{2v}$ (bent) geometry, a $UH_3$ molecule adopted a $C_3$ (pyramidal) geometry, and a $UH_4$ molecule adopted a $T_d$ (tetrahedral) geometry. In this study, the uncharged $UH_2$ molecule also adopts a $C_{2v}$ geometry with bond lengths of 2.213 Å and a H-U-H angle of 109.1°, while the uncharged $UH_4$ molecule adopts a square planar arrangement with U-H 2.172 Å and H-U-H angles of 89.5° - 90.5°, compared to the *Souter et al* [11] 1.991 Å and 105° for $UH_2$ and a tetrahedral $UH_4$ with U-H = 1.979 Å. These apparent discrepancies can be explained by the different functionals used; in this work PBE [10] and *Souter et al* [11] *Becke88* exchange gradient correction [12] and *Perdew86* correlation correction [13]. The results with the PBE functional in this work appear to be in better agreement with experiment as judged by vibrational frequencies (*vide subra*).

The square planar geometry of the negatively charged ions is due to the greater involvement of the 6*d* orbitals in the U-H bonding. When the $UH_4^+$ ion was optimised starting from a tetrahedral geometry a $UH_2^+$ ion with a loosely bound $H_2$ molecule was obtained, as shown in Figure 6, indicating that the $UH_4^+$ ion is unstable with respect to dissociation of $H_2$ with a low activation barrier. The fate of the $UH_4^+$ ion is confirmed when the electronic energies are compared and the change in energy computed for the dissociation of the molecular ions. For the $UH_x^+$ molecular ions with $x > 2$, the calculations indicate that all are unstable with respect to dissociation to $UH_{x-1}$ + H, or $UH_{x-2}$ + $H_2$. This is consistent with the species observed in the ToF-SIMS reported here, with $U^+$ and $UD^+$ detected, but with the higher cationic uranium deuteride ions absent. The $UH_x^-$ ions, however,

are calculated to be stable with respect to dissociation into $UH_{x-2}^-$ + $H_2$, and $UH_{x-1}^-$ + H, which is also in agreement with the ToF-SIMS reported here, in which $UD_x^-$ ions up to x = 4 are detected.

In addition to examining the sites where deuteride was observed to have formed, a more general study was undertaken with ToF-SIMS to examine the $D_2$ exposed uranium surface for evidence which might explain why certain sites will preferentially nucleate hydride. Many SIMS images were examined for evidence of patterns within the deuterium containing ion fragments, such as images where these signals might follow the visually observable grain structure. However, despite much time being dedicated to this study no convincing trends were uncovered; either offering support for, or against, preferential grain boundary versus lattice diffusion theories. Further, more careful investigation is required on this matter before any final conclusions can be drawn.

During the ToF-SIMS investigation of the $D_2$ exposed uranium surface a suspected carbide inclusion site was identified and examined, the images of which are shown in figure 7. The uranium carbide/oxy-carbide family of compounds have their structures based around the NaCl structure [14], and are often observed as square in appearance on polished samples. Figure 7 (total) shows the inclusion as a dark square feature approximately 20 μm across in the centre of the image. By examining differences in timing between ions collected from the 20 μm across inclusion region and ions from the adjacent areas, the carbide feature is proven to be slightly lower in height than the surrounding oxide [15]. The inclusion region was DC sputtered to a depth of 120 Å (according to SRIM calculations) to remove the surface oxide before the remaining data in figure 7 ($UO_2^+$, $U^+$, $UC^+$, $C^-$, $UD^-$, $UD_2^-$, $UB^-$) were captured.

Studying figure 7 ($UO_2^+$, $U^+$, $UC^+$, $C^-$) it can be seen that the inclusion, as suspected, is indeed a particle containing both uranium and carbon atoms. Significant $UN^+$ signals were also detected from the inclusion, but are not shown

in the figure. However, figure 7 ($UB^-$) reveals that this particle does in fact appear to contain boron in addition to uranium and carbon. A positive ion peak was observed at m/z = 11 from the inclusion, which would appear to confirm the presence of boron. Moreover, the negative ion SIMS spectra from the inclusion (not shown) not only shows a peak at m/z = 249 ($U^{11}B^-$), but also a peak at m/z = 248 ($U^{10}B^-$) which appears at approximately one fifth of the signal intensity. The natural abundance of $^{10}B$ when compared to $^{11}B$ isotope is approximately 1:4 [16], adding further support to the assignment of m/z = 249 to UB. $UB_2$ is the stable phase expected to form in uranium material containing sufficient boron [17]. Figure 7 ($U^+$, $UC^+$, $C^-$, $UB^-$) clearly show that the distribution of uranium, carbon and boron is not even across the inclusion, although each of the three elements is clearly more prevalent in the inclusion region than in the surrounding areas. The extended heat treatment periods experienced during manufacture of this coupon were intended to result in a larger grain size. However, this process may have also resulted in the formation of inclusions such as the one observed in figure 7, through the increased diffusion of carbon, nitrogen and boron. The existence of ternary phases such as UBC or $UB_2C$ appears unlikely in a material which is almost pure uranium; however it is possible that the inclusion is a combination of UC, UN and $UB_2$, with the co-existence of such phases being due to the site acting as a nucleation point within the high purity metal.

Examining figure 7 ($UD^-$, $UD_2^-$) evidence exists which appears to show either initial deuteride formation, or preferential $D_2$ diffusion around the edges of the inclusion site. To explain the reasons for preferential deuterium diffusion around the edges of the inclusion we must first remember the earlier ToF-SIMS timing result, which demonstrated that the inclusion is lower in height than the surrounding oxide. This result is in agreement with our understanding, since uranium oxide grows via anion diffusion [18] and $UO_2$ is less dense than uranium metal [7]; it is therefore expected that the inclusion will appear lower than the oxide layer which has grown upwards around it. The resultant effect is that around the edge of inclusions such as that observed in figure 7, there will be a

reduced thickness of $UO_2$ for hydrogen species to diffuse through, and thus the reaction between hydrogen and the underlying metal will have an increased probability. These factors explain why preferential deuterium diffusion, and possibly deuteride growth can occur around the edges of this inclusion site. *Owen* and *Scudamore* identify carbide inclusions as sites which can initiate hydride formation on uranium surfaces exposed to hydrogen [6]. Much of the literature on uranium hydriding describes the spot-wise appearance of hydride sites as due to discontinuities, defects, or oxide film deficiencies in the region of the attack. As discussed above, the thickness of the oxide formed on the uranium coupon should be reduced around the edges of an inclusion. Stress exerted at the oxide / inclusion interface by the growth of the oxide layer around the inclusion might also result in cracking, which in turn would be expected to further increase the hydrogen diffusion rate around an inclusion site.

The $UD^-$ signal in figure 7 could also be interpreted as $UH_2^-$, and the $UD_2^-$ signal as $UH_4^-$. In this case it means that evidence of hydride formation is being observed around the inclusion, however not from the $D_2$ exposure undertaken here, but from hydrogen already present within the uranium metal. Therefore, the results in figure 7 could be interpreted as coming from hydrogen within the metal lattice, but beyond the solubility limit, nucleating $UH_3$ at the inclusion site. If this were the case then the hydride evidence observed at the inclusion site would have existed long before the exposure to deuterium occurred within this experiment, and in fact the hydride would have been present since the metal sample cooled after casting.

DFT calculations were employed to examine the $UO_2^{2+}$, $UO_2^+$, $UO^+$, $UOF^+$, $UC^{+/-}$ and $UB^{+/-}$ molecular ions (Figure 8), with $UO_2$ chosen for direct comparison with experimental studies and other theoretical calculations. In this study, the calculated U=O bond length, 1.756 Å, is slightly longer (0.05 Å) than some literature values [19] notably that calculated using the B3LYP functional [20]. A frequency calculation on the $UO_2^{2+}$ cation yields a Raman absorption at 839 $cm^{-1}$

which again compares very favourably with the experimental value of 870 $cm^{-1}$ [21], while the equivalent B3LYP calculation in the literature arrived at a Raman frequency of 975 $cm^{-1}$ [19]. These results serve to reinforce our choice of functional, and validate the calculated results obtained for the uranium hydride ions (*vide supra*).

In the case of the $UX^{+/-}$ ions (where X = C or B) the trend in U-X bond length is opposite to that observed earlier for the $UH_x$ ions. When X = C or B the negatively charged ions display shorter bond lengths than observed for the positively charged ions. The calculations indicate that, while the $UB^-$ anion is stable with respect to dissociation, the $UB^+$ cation is unstable with respect to dissociation into $U^+$ + B. This result is again in complete agreement with the SIMS data, where $UB^-$ is clearly observed, but no $UB^+$ intensity is found. From the calculations undertaken in this work both the anion and cation of UC appear stable with respect to dissociation, which again agrees well with the SIMS data.

## Conclusions

ToF-SIMS has been employed to examine a depleted uranium coupon after exposure to high purity $D_2$ gas. The $D_2$ gas exposure resulted in $UD_3$ formation at discrete sites over the surface of the polished uranium coupon. The ToF-SIMS images captured from a $UD_3$ site are the first of their kind reported in the literature. DFT calculations have been performed, which confirm the stability of the various uranium containing ions observed with SIMS, and also assign structural geometries to the ion fragments. The calculations show that $UH_2^{+/-}$ ions adopt a linear arrangement, while $UH_3^+$ and $UH_4^+$ ions adopt structures based on a tetrahedral geometry, and $UH_3^-$ and $UH_4^-$ ions adopt structures based on a square planar geometry. SIMS measurements show that although a subsequent uranium oxide film formed over the $UD_3$ reaction sites after exposure to air at room temperature, the 300 μm in diameter deuteride site was not completely oxidised, but instead a protective oxide cap formed, estimated through SRIM calculations to be approximately 200 Å thick. ToF-SIMS images

were collected from across the uranium coupon surface in an attempt to prove grain boundary diffusion as the dominant transport medium for hydrogen species traversing the oxide during hydride formation; no conclusive evidence was found to prove this hypothesis. An inclusion site observed at the surface of the polished uranium coupon was also investigated by ToF-SIMS, and evidence suggests that the edges of such inclusion sites exhibit increased D ion, and hence H ion, diffusion when compared to the surrounding surface oxide. These results support the previously published hypotheses [6] that carbide sites on uranium metal surfaces exhibit an increased probability to form hydride under exposure to hydrogen.

**Acknowledgements**

Rick Gross (LLNL) is acknowledged by the authors for his diligent sample preparation work and Tom Felter (LLNL) is thanked for his SRIM sputtering calculations for $UO_2$. This work was performed under the auspices of the U.S. Department of Energy by the University of California Lawrence Livermore National Laboratory under Contract No. W-7405-Eng-48.

**References**

[1] J.J. Katz, E. Rabinowitch, The Chemistry of Uranium – collected papers, United States Atomic Energy Commission, second ed., 1958, pp 183.

[2] D. Moreno, R. Arkush, S. Zalkind, N. Shamir, J. Nuc. Mater 230 (1996) 181.

[3] M. Brill, J. Block, M.H. Mintz, J. Alloys Comp. 266 (1998) 180.

[4] R. Arkush, A. Venkert, M. Aizenshtein, S. Zalkind, D. Moreno, M. Brill, M.H. Mintz, N. Shamir, J. Alloys Comp. 244 (1996) 197.

[5] J.F. Bingert, R.J. Hanrahan Jr, R.D. Field, P.O. Dickerson, J. Alloys Comp. 365 (2004) 138.

[6] L.W. Owen and R.A. Scudamore, Corrosion Sci. 6 (1966) 461.

[7] A.N. Holden, physical Metallurgy of uranium, Addison Wesley, Reading, MA, 1958, pp. 220-223.

[8] J.B. Condon, E.A. Larson, J. Chem. Phys. 59 (1973) 855.

[9] Gaussian 03, Revision C.02, M.J. Frisch, G.W. Trucks, H.B. Schlegel, G.E. Scuseria, M.A. Robb, J.R. Cheeseman, J.A. Montgomery Jr., T. Vreven, K.N. Kudin, J.C. Burant, J.M. Millam, S.S. Iyengar, J. omasi, V. Barone, B. Mennucci, M. Cossi, G. Scalmani, N. Rega, G.A. Petersson, H. Nakatsuji, M. Hada, M. Ehara, K. Toyota, R. Fukuda, J. Hasegawa, M. Ishida, T. Nakajima, Y. Honda, O. Kitao, H. Nakai, M. Klene, X. Li, J. E. Knox, H.P. Hratchian, J.B. Cross, C. Adamo, J. Jaramillo, R. Gomperts, R.E. Stratmann, O. Yazyev, A.J. Austin, R. Cammi, C. Pomelli, J.W. Ochterski, P.Y. Ayala, K. Morokuma, G.A. Voth, P. Salvador, J.J. Dannenberg, V.G. Zakrzewski, S. Dapprich, A.D. Daniels, M.C. Strain, O. Farkas, D.K. Malick, A.D. Rabuck, K. Raghavachari, J.B. Foresman, J.V. Ortiz, Q. Cui, A.G. Baboul, S. Clifford, J. Cioslowski, B.B. Stefanov, G. Liu, A. Liashenko, P. Piskorz, I. Komaromi, R.L. Martin, D.J. Fox, T. Keith, M.A. Al-Laham, C.Y. Peng, A. Nanayakkara, M. Challacombe, P.M.W. Gill, B. Johnson, W. Chen, M.W. Wong, C. Gonzalez, and J.A. Pople, Gaussian, Inc., Wallingford CT, (2004).

[10] J.P. Perdew, K. Burke and M. Ernzerhof, Phys. Rev. Lett. 77 (1996) 3865; *ibid idem*, 78 (1997) 1396.

[11] P.F. Souter, G.P. Kushto, L. Andrews and M. Neurock, J.Am.Chem.Soc. 119 (1997) 1682.

[12] A.D. Becke, Phys. Rev. A. 38 (1988) 3098.

[13] J.P. Perdew and Y Wang, Phys. Rev. B. 33 (1986) 8822.

[14] P.E. Potter, J. Nuc. Mater. 42 (1972) 1.

[15] ToF-SIMS data are very sensitive to the z position (or height) of the sample, since changes in z position have the effect of changing the flight tube length for the secondary ions emitted from the surface. Comparing timing changes for identical m/z components occurring from different areas across the

samples can elucidate the relative height differences between specific areas under examination.

[16] Isotopic Compositions of the Element, Pure and Applied Chemistry, 70 (1998) 217.

[17] P. Rogl, J. Bauer and J. Denuigne, J. Nuc. Mater. 165 (1989) 74.

[18] H. Matzke, J. Nuc. Mater. 114 (1983) 121.

[19] Y. Oda and A. Aoshima, J. Nucl. Sci. Tech. 39 (2002) 647.

[20] A.D. Becke, J. Chem. Phys. 98 (1993); S.H. Vosko, L. Wilk, M. Nusair, Can. J. Phys. 58 (1980) 1200C. Lee, W. Yang and R.G. Parr, Phys. Rev. B 37 (1988) 785.

[21] C. Nguyen-Trung, G.M. Begun, D.A. Parker, C. Peiffert and R.E. Mesmer, Inorg. Chem. 31 (1992) 5280; L.M. Toth and G.M. Begun, J. Phys. Chem. 85 (1981) 547.

**Captions**

Table 1 The calculated ion energies of $UH_x^{+/-}$ fragments (where x = 1 to 4), and selected uranium anions and cations containing oxygen, carbon, boron and fluorine. Only the energy of the lowest spin state is quoted in each case, with the multiplicity given in brackets. † Not computed.

Figure 1 An optical microscope image of the major deuteride spot investigated with the ToF-SIMS. The picture is captured after the $D_2$ gas has been evacuated from the reaction cell, but before the sample was exposed to air and moved into the SIMS instrument. It should be noted that the image must be rotated 45° counter-clockwise in order to obtain the same orientation as images taken with the SIMS (figure 2).

Figure 2 Showing eight 300 × 300 μm ToF-SIMS images, four positive and four negative, of the deuteride site studied in figure 1. The scale bars in the images are 100 μm in length. All the images (except total) were captured after two 50 × 50 μm regions were sputter etched into the sample, the first positioned towards the top left of each image and the second positioned atop of the deuteride feature. The total image was collected prior to sputtering the sample. The brightness within each image relates directly to the intensity of the imaged ion fragment.

Figure 3 Showing the SIMS spectra obtained from outside the deuteride region (top), and directly from above the deuteride region (bottom). Both spectra show the characteristic secondary ion fragments expected from $UO_2$; m/z = 238 ($U^+$), 254 ($UO^+$) and 270 ($UO_2^+$). Additional lines are also observed which relate to recombination of $UO_2$ fragments with hydrogen and fluorine ions.

Figure 4 Showing both the positive (bottom) and negative (top) SIMS spectra obtained from deuteride, after exposure by sputtering. Ion fragments characteristic of $UD_3$ formation are observed at m/z = 238 ($U^+$), 240 ($UD^+$), 242 ($UD_2^-$), 244 ($UD_3^-$) and 246 ($UD_4^-$). Additional mass fragments are observed due to the combination of $UD_3$ ions with available oxygen ions.

Figure 5 Showing the calculated geometries of the $UH^{+/-}$, $UH_2^{+/-}$, $UH_3^{+/-}$, and $UH_4^{+/-}$ ions. Note that the $UH_2^{+/-}$ ions adopt a linear arrangement, while $UH_3^+$ and $UH_4^+$ ions adopt structures based on a tetrahedral geometry, and $UH_3^-$ and $UH_4^-$ ions adopt structures based on a square planar geometry.

Figure 6 The calculated minimum energy configuration of the $UH_4^+$ cation when initially starting from a tetrahedral ($T_d$) geometry. Here the $UH_4^+$ ion dissociates to form $UH_2^+ + H_2$.

Figure 7 Showing eight 50 × 50 μm ToF-SIMS images, four positive and four negative, of a surface carbide inclusion after exposure to $D_2$. The scale bars in the images are 10 μm in length. All the images (except total) were captured after the carbide region was sputter etched to remove the surface oxide and fully expose the feature. The total image was collected prior to sputtering the sample. The brightness within each image relates directly to the intensity of the imaged ion fragment.

Figure 8 Showing the calculated geometries of the $UO_2^+$, $UO^+$, $UB^{+/-}$, $UC^{+/-}$ and $UOF^+$ ions.

**Table 1**

| Molecular ion | Anion Energy (Ha) | Cation Energy (Ha) |
|---|---|---|
| UH | -52.10974505 (septet) | -52.01092257 (quintet) |
| $UH_2$ | -52.75562857 (sextet) | -52.56582246 (quartet) |
| $UH_3$ | -53.38867110 (quintet) | -53.08583205 (triplet) |
| $UH_4$ | -53.994762242 (quartet) | -53.59674170 (doublet) |
| $UH_4$ (as $UH_2$+$H_2$) | | -53.6949447 (doublet) |
| UB | -76.2922229 (triplet) | -76.03695076 (triplet) |
| UC | -89.53069667 (quartet) | -89.313118 (doublet) |
| $UO_2$ | n/c† | -201.80650770 (doublet) |
| UOF | n/c† | -226.45266797 (triplet) |
| UO | n/c† | -126.6326596 (quartet) |

**Figure 1**

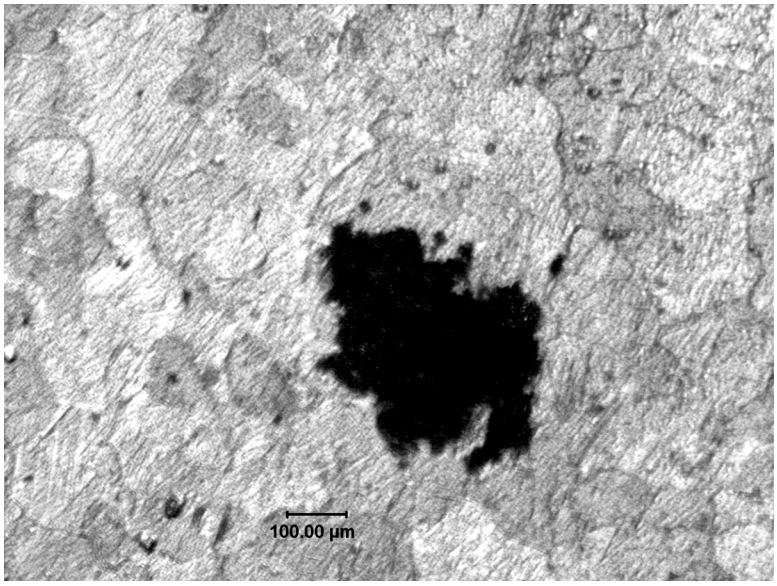

**Figure 2**

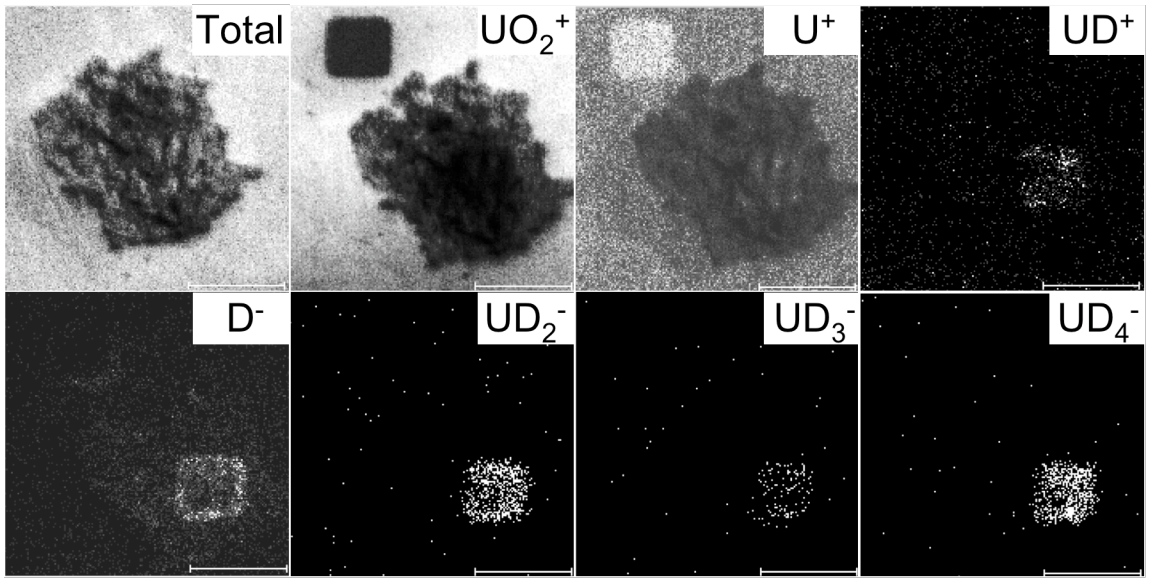

**Figure 3**

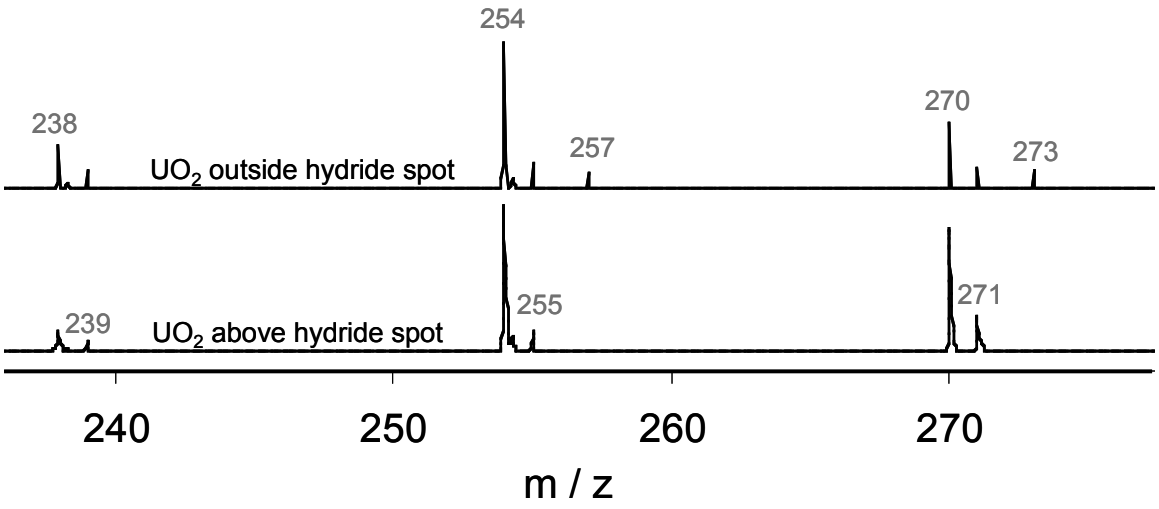
254
238
257
270
273
UO2 outside hydride spot
239
255
271
UO2 above hydride spot
240
250
260
270
m / z

**Figure 4**

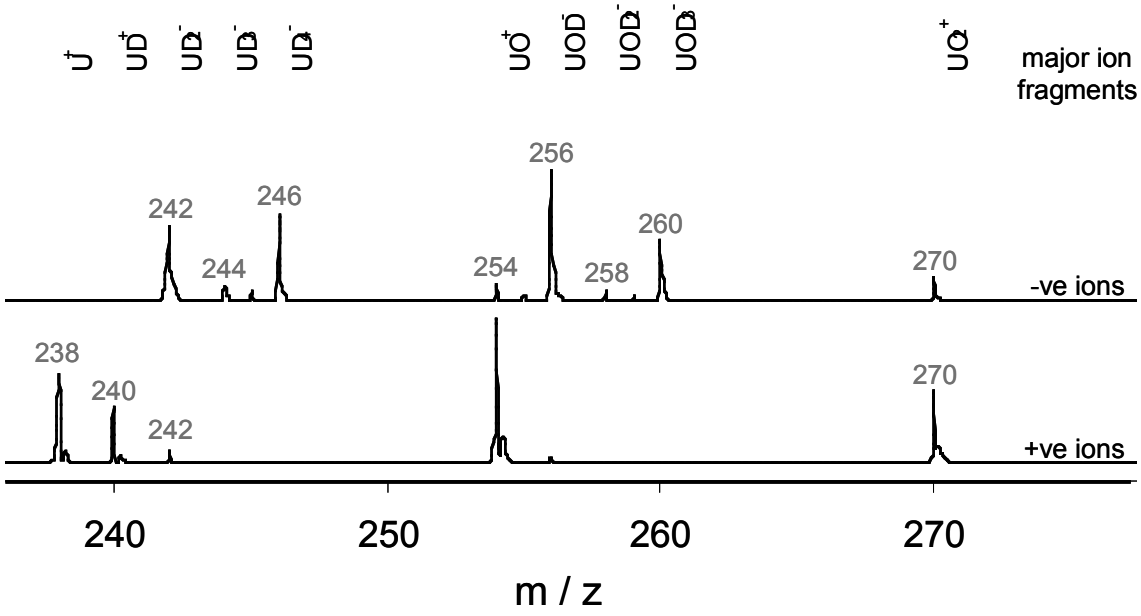
U+
UD+
UD2-
UD3-
UD4-
UO+
UOD-
UOD2-
UOD3-
UO2+
major ion fragments
256
242
246
260
244
254
258
270
-ve ions
238
240
242
270
+ve ions
240
250
260
270
m / z

**Figure 5**

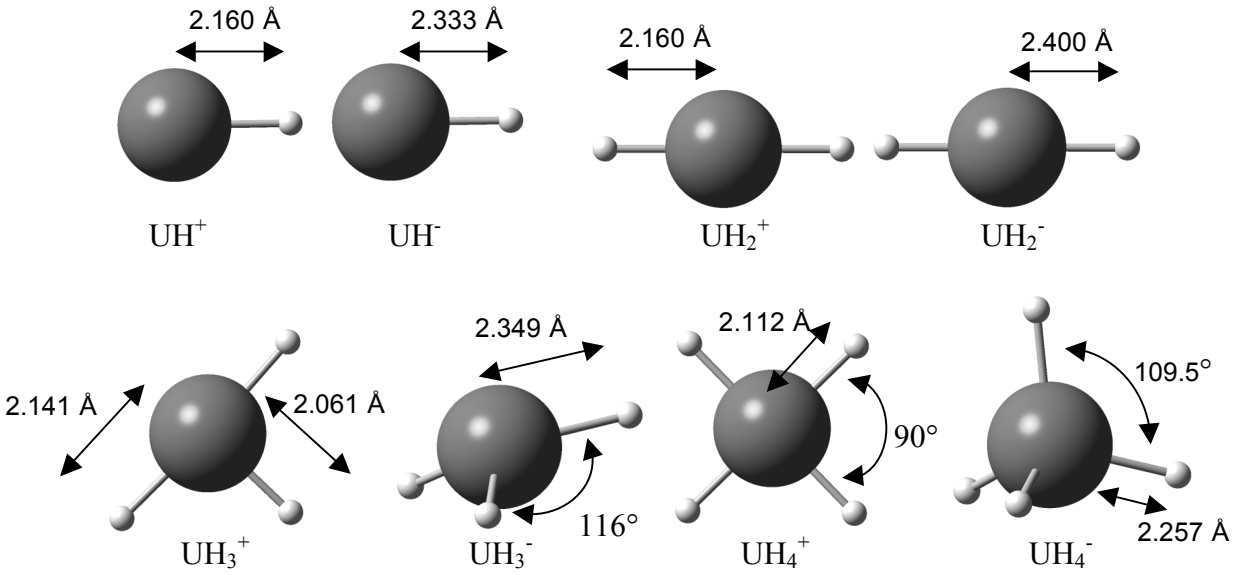
2.160 Å
2.333 Å
2.160 Å
2.400 Å
UH+
UH-
UH2+
UH2-
2.141 Å
2.061 Å
2.349 Å
2.112 Å
109.5°
90°
116°
2.257 Å
UH3+
UH3-
UH4+
UH4-

**Figure 6**

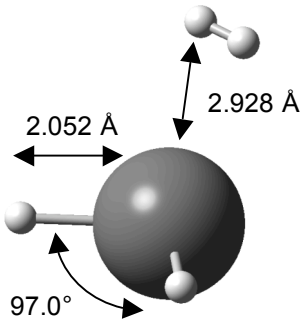

**Figure 7**

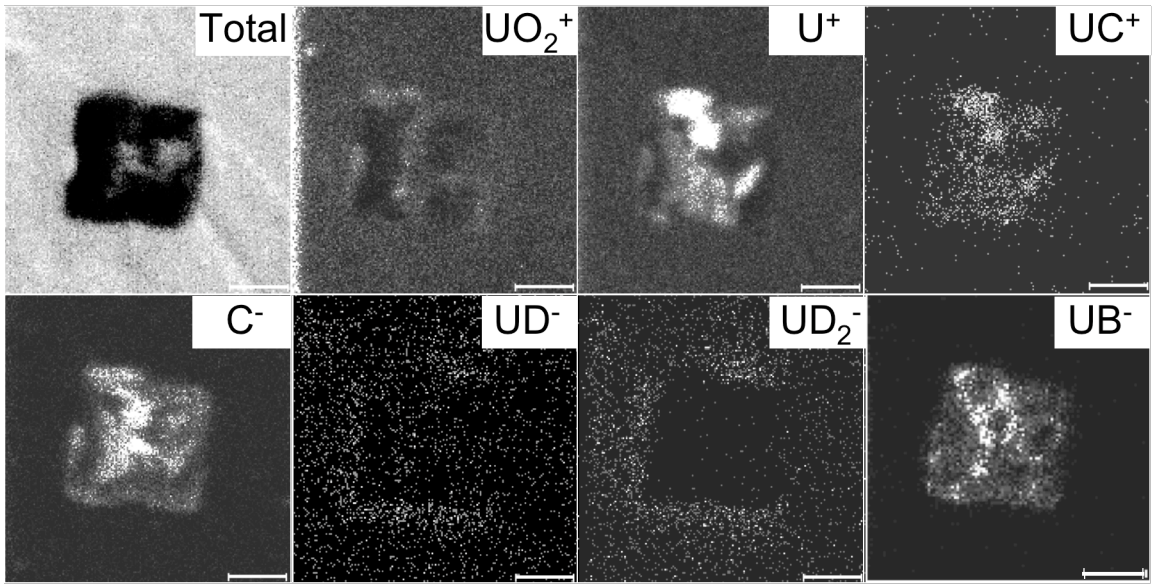

**Figure 8**

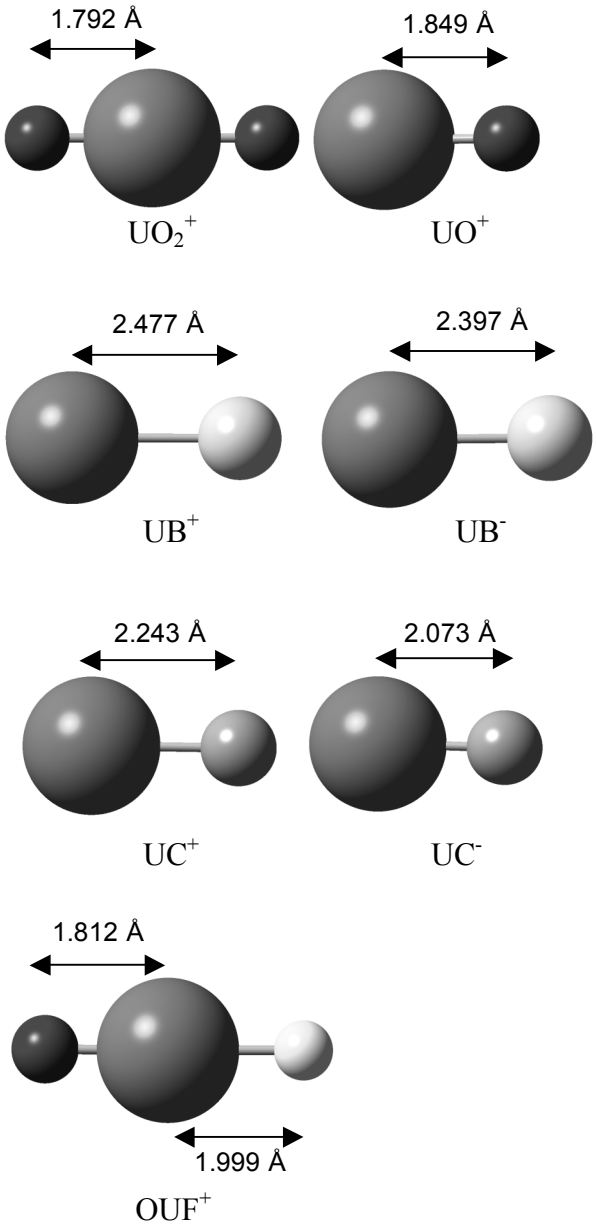
1.792 Å
1.849 Å
$UO_2^+$
$UO^+$
2.477 Å
2.397 Å
$UB^+$
$UB^-$
2.243 Å
2.073 Å
$UC^+$
$UC^-$
1.812 Å
1.999 Å
$OUF^+$